COMMENT

WILEY

Practical challenges of continuous real-time functional magnetic resonance imaging neurofeedback with multiband accelerated echo-planar imaging and short repetition times

Malika P. Renz[1] | Francesca Zidda[1] | Jamila Andoh[1] | Marcel Prager[2] | Markus Sack[3,4] | Robert Becker[3,4] | Matthias Ruf[3,4] | Mike M. Schmitgen[5] | Robert C. Wolf[5] | Andreas Meyer-Lindenberg[1] | Heike Tost[1]

[1]Department of Psychiatry and Psychotherapy, Medical Faculty Mannheim, Central Institute of Mental Health University of Heidelberg, Mannheim, Germany

[2]Department of Neuroradiology, Heidelberg University Hospital, Heidelberg, Germany

[3]Department of Neuroimaging, Medical Faculty Mannheim, Central Institute of Mental Health, University of Heidelberg, Mannheim, Germany

[4]Center for Innovative Psychiatry and Psychotherapy Research, Medical Faculty Mannheim, Central Institute of Mental Health, University of Heidelberg, Mannheim, Germany

[5]Department of General Psychiatry, Center for Psychosocial Medicine, Heidelberg University, Heidelberg, Germany

Correspondence
Heike Tost, Department of Psychiatry and Psychotherapy, Medical Faculty Mannheim, Central Institute of Mental Health University of Heidelberg
Mannheim, Germany.
Email: heike.tost@zi-mannheim.de

Abstract

Continuous real-time functional magnetic resonance imaging (fMRI) neurofeedback is gaining increasing scientific attention in clinical neuroscience and may benefit from the short repetition times of modern multiband echoplanar imaging sequences. However, minimizing feedback delay can result in technical challenges. Here, we report a technical problem we experienced during continuous fMRI neurofeedback with multiband echoplanar imaging and short repetition times. We identify the possible origins of this problem, describe our current interim solution and provide openly available workflows and code to other researchers in case they wish to use a similar approach.

KEYWORDS

fMRI neurofeedback, image recostruction, imaging, multiband echo-planar, repetition time, self-regulation training

1 | INTRODUCTION

Real-time functional magnetic resonance imaging (fMRI) neurofeedback experiments enable individuals to learn to self-regulate certain brain activation or connectivity patterns by monitoring a feedback signal and devising a strategy to modify it (Sitaram et al., 2017). The influence of key protocol parameters on learning outcomes is currently under debate (Linhartova et al., 2019; Oblak et al., 2017),

especially the impact of different self-regulation strategies and feedback timings (continuous vs. intermittent). Continuous fMRI neurofeedback protocols update the feedback signal after each brain scan or repetition time (TR). This results in a temporal resolution of the feedback signal of 0.5 Hz in most current studies with whole-brain coverage. Modern multiband echo-planar imaging (MB-EPI) sequences offer a significant increase in image sampling rate. This is relevant to real-time fMRI neurofeedback because higher temporal resolution

allows investigation of the role of feedback signal continuity in self-regulation learning and may increase the signal-to-noise ratio (SNR) and reliability of connectivity feedback signals. Here, we report technical challenges with such a neurofeedback scanning protocol, detail our workaround, and discuss the causes.

2 | EXPERIENCED CHALLENGES

We collected fMRI data using a 3 T Siemens Prisma^fit scanner with Windows 7-based VE11C console software at the Central Institute of Mental Health (CIMH), Mannheim, using a 64-channel head coil (Siemens) and an MB-EPI sequence developed at the Center for Magnetic Resonance Research (CMRR), University of Minnesota (Release R016a) with TR = 800 ms, MB factor 6, field of view (FOV) = 204 mm, voxel size 2.4 mm^3 and 60 slices. We provide further details on the sequence parameters and technical specifications in Table 1 and Supplementary Information S1. During experiments, we presented images of negative affective scenes from the International Affective Picture System (Bradley & Lang, 2007) and provided adaptively scaled, continuous visual feedback of the blood oxygenation level-dependent signal from the right amygdala via a thermometer display. Following an established workflow (Paret et al., 2018), we defined the region of interest, preprocessed the images, and computed the feedback values using SPM12 and Matlab R2018b on a laptop connected to the scanner host PC via Ethernet (TCP/IP). The

scanner host was configured to forward the output of the measurement and reconstruction system (MaRS) directly to a shared network folder on the laptop. Upon calculation, feedback scores were transmitted from the laptop to a stimulus presentation computer, which updated the thermometer display with each incoming data bin. Figure S1 shows an overview of the setup's hardware components, connections, and data streams.

We observed anomalies during real-time image processing on the laptop in the form of unexpected Matlab crashes. Code profiling and examination of DICOM header data suggested irregular image arrival times in the network folder. We confirmed this by running a minimal version of the feedback script, reduced to monitoring image arrivals. During these measurements, we noted two qualitatively different phases of irregular image arrival times that we refer to as "initial chaotic phase" and "semistable phase," respectively (Figure 1a).

The initial chaotic phase was characterized by a long delay in the arrival of the first image file followed by highly irregular image arrival intervals with abrupt switches between delayed (>1 TR) and nearly instantaneous arrival times of images, including instances of two or more consecutive image files arriving simultaneously. A similarly chaotic display of incoming mosaic files in real-time was also apparent on the MR host display. In the semistable phase, there were fewer instances of near-simultaneous delivery but the time intervals between two consecutive image arrival times remained irregular until the end of the scan. K-means clustering suggested two distinctive time bins for the initial chaotic phase and three time bins for the semistable phase (Figure 1b). Absolute delays (i.e., time differences between scanner trigger pulses and the image arrivals) mirrored these irregularities (Figure S2).

3 | SEARCHING FOR CLUES

We performed several plausibility checks to narrow down the cause of the issue. First, we repeated the measurements with the same MB-EPI sequence specifications on a second Prisma^fit scanner with a Windows 7-based operating system. Despite differences in the hardware and software (Table 1), we detected similar irregularities in image arrivals, including the initial chaotic and semistable phases and clustering into characteristic time bins described above (Figure 1c, d).

Second, we repeated the measurements on the first Prisma^fit scanner using a Siemens product sequence with comparable settings (TR = 800 ms, SMS factor 6, FOV = 204 mm, voxel size 2.4 mm^3, 54 slices; Supplementary Information S2). We observed no initial chaotic phase with the Siemens sequence but more frequent and much longer (>1.5 s) occasional delays in image arrivals in the semistable phase (Figure 1e,f).

Third, we tested the effects of successive TR increases (range: 800 ms to 2000 ms) using the CMRR MB-EPI sequence with otherwise identical settings (Tables S3–S14). Here, image arrival times in the initial chaotic phase remained irregular and highly variable (Figure 2, upper panel) while those in the semistable phase became more uniform with increasing TR up to a value of 1000 ms, where a
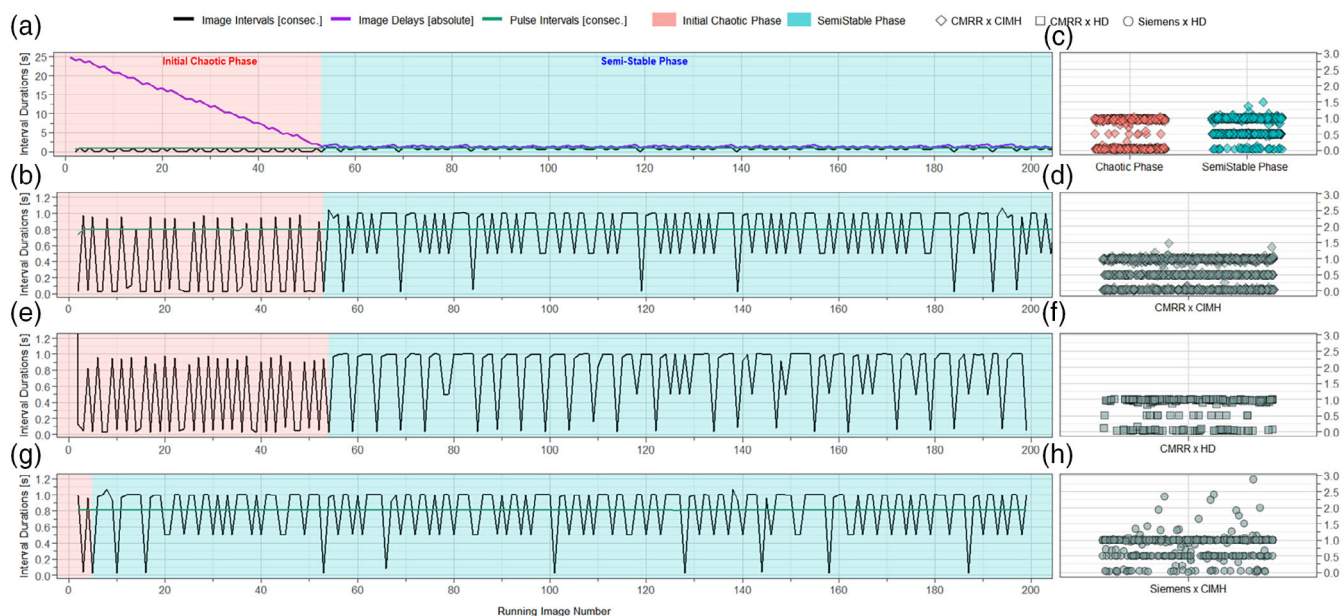
TABLE 1 Technical specifications of MRI scanners used

	Site 1: Central Institute for Mental Health	Site 2: Heidelberg University Hospital
Scanner	Siemens Magnetom Prisma Fit	Siemens Magnetom Prisma Fit
• Software	VE11C	VE11E
• Head Coils	Siemens Head/Neck 64, Head 32, Head/Neck 20	Siemens Head/Neck 64
MaRS	2D.2128 RX	3D.3_2 128RX
• CPU	2× Intel Xeon E5-2690 8C/16 T 2.9 GHz	2× Intel Xeon E5-2640v4 10C/20 T 2.4 GHz
• RAM	16 × 8 GB DDR3L-1600	8 × 16 GB DDR4-2666
• GPU	1 Nvidia Tesla K10 graphics card with 2 chips: 2× GK104 (2 × 1536 Cores) 2× 4 GB memory	2 Nvidia Quadro P4000 graphics cards with 1 chip: 2× GP104 (1792 Cores) 2 × 8 GB memory
• Storage	1800 GB total; 6 × 300 GB 10 K SATA	3120 GB total; 1 × 240 GB SSD SATA 6 × 480 GB SSD SATA
Network	1 Gbit/s	1 Gbit/s

Abbreviation: MRI, magnetic resonance imaging.

FIGURE 1 Timing of image file arrivals at repetition time = 800 ms using different scanners and sequences. (a,b) Irregularities in intervals between image file arrivals (black line) using a Center for Magnetic Resonance Research (CMRR)-based MB(6)-echo-planar imaging sequence at the Central Institute of Mental Health (CIMH). Absolute delays of image file arrivals (purple line) calculated as time passed since the respective MR pulse (green line). Initial chaotic and semistable phases ((light red and blue) as determined by time series changes in mean and SD and by linear fitting of absolute delays. (c,d) K-means clustering of intervals between image file arrivals reveals two clusters for the initial chaotic phase and three clusters for the semistable phase resulting in three stable clusters for all CMRR × CIMH measures (diamonds). (e,f) CMRR × HD replication (squares) using identical sequence at a different Prismafit scanner at university hospital Heidelberg, for technical specifications of both scanners see Table 1. (g,h) Siemens × CIMH replication (circles) using a Siemens product sequence with parameters matching as closely as technically possible, see Supplementary Material S1 and S2 for sequence details
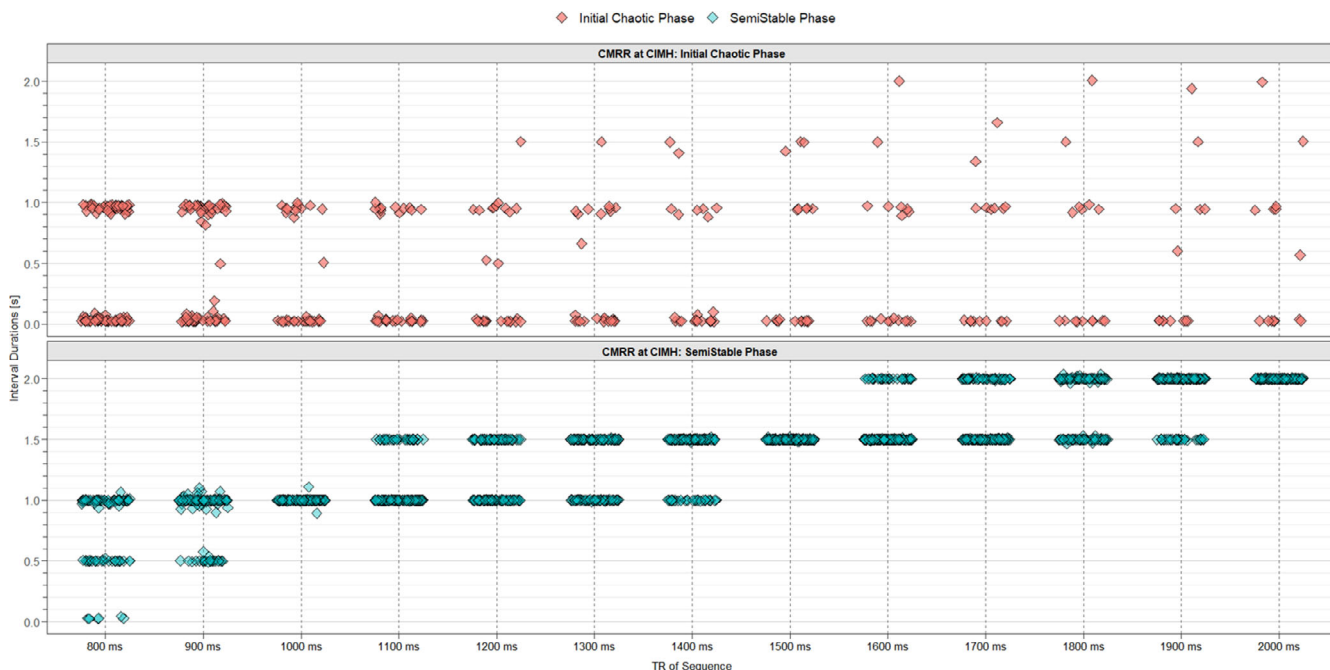

FIGURE 2 Timing of image file arrivals by phase at different repetition time (TRs) using the Center for Magnetic Resonance Research (CMRR)-based MB(6)-echo-planar imaging sequence at Central Institute of Mental Health (CIMH). Upper panel: Intervals between consecutive image files arriving remain highly irregular during the chaotic phase (light red) irrespective of TR. Lower panel: During the semistable phase (light blue), a constant evenlyspaced stream of images is achieved at TRs of 1000, 1500, and 2000 ms but not at any TR that is not a multiple of 500 ms.

TABLE 2 Effect of sequence modifications on image arrival times

	Baseline[a] settings	MB LeakBlock kernel = OFF	Matrix optimization = ON	32-channel head coil	Matrix size = 74
Initial Chaotic Phase: Duration [s, TR]	≈57.5 s (72 TR)	≈14.5 s (18 TR)	≈17 s (21 TR)	≈21.5 s (27 TR)	≈25.5 s (32 TR)
Initial Chaotic Phase: duration reduction [%]	—	74.8%	70.4%	62.6%	55.7%
Variability of image arrivals in semistable phase (SD, [s])	0.272	0.259	0.255	0.266	0.3015

Abbreviations: CMRR, Center for Magnetic Resonance Research; EPI, echo-planar imaging; FOV, field of view; TR, repetition time.
[a]CMRR-based MB(6)-EPI, TR = 800 ms, FOV = 204 mm, voxel size 2.4 mm³, 64-channel head coil, matrix size = 84, number of slices = 60.

stable stream of incoming images was observed (99% CI for mean interval duration = 0.997–1.002). Surprisingly, irregular image arrival times in the semistable phase reappeared at TRs of 1100, 1200, 1300, 1400, 1600, 1700, 1800, and 1900 ms. In contrast, we observed constant image arrivals at TR settings of 1000, 1500, and 2000 ms (Figure 2, lower panel).

Fourth, we tested the effects of various modifications to the protocol parameters (Tables S20–S32). Modifications that reduced the computational cost of reconstructing the first image (e.g., matrix size reduction, MB LeakBlock kernel = off, Table 2) shortened the initial chaotic phase by 56%–75% but did not affect irregularities in the semistable phase. Finally, we monitored the CPU and GPU load on the MaRS while running the CMRR MB-EPI sequence with the original presets. Here, we only noticed an initial increase in CPU load during the reconstruction of the first image which rapidly returned to normal.

4 | INTERIM SOLUTION

We currently use a TR of 1000 ms, the shortest possible TR meeting both the requirements of our experiment (higher temporal resolution, whole-brain coverage, continuously updated feedback at constant intervals) and our scanning system's constraints. To circumvent the initial chaotic phase, we further adjusted our neurofeedback code to ignore the first 120 images (corresponding to the mean length + 3 SD of the initial chaotic phase) and unusually small image files. This allowed us to halve our previous feedback intervals and to collect data from 120+ subjects to date without any problems. Our procedures and code are publicly available here: https://doi.org/10.11588/data/AIGXZZ.

5 | SUMMARY ASSESSMENT

The observed problem occurred on two independent Siemens Prisma-fit scanners, arguing against a scanner-specific problem. While the pronounced variability in image arrival times during the initial chaotic phase appears to be related to the MB-requirements of the CMRR sequence, irregularities in image delivery during the semistable phase

also occurred when using the Siemens product sequence, arguing against a sequence-specific problem. Overall, we assume that two different causes take effect here.

First, in the "semistable phase," irregular image arrivals reappeared at TRs over 1000 ms and were limited to TRs that did not correspond to a multiple of 500 ms, arguing against a hardware bottleneck. This, and helpful advice from Siemens engineers and reviewers helped narrow down the problem: The console platforms of both Prisma^Fit scanners are equipped with a Windows 7-based operating system only supporting an older version (2.x) of the Server Message Block (SMB) protocol required to exchange data with the real-time processing laptop. Older SMB versions are slower and incur more overhead than newer protocol versions (e.g., SMB 3.3, see also Lührs et al., 2022). Especially when using outdated devices (e.g., Windows XP-based computers supporting only SMB versions 1.x), this could lead to such massive delays that even neurofeedback experiments with intermittent feedback may be affected. Here, port-forwarding ("tunneling") through the console may help to mitigate the issue.

Additionally, the sampling rate of new images to be processed is internally set to 500 ms by the configuration software (ideacmdtool option "SendBuffered = off"), which may contribute to irregular image arrivals if the TR is not a multiple of this rate. Notably, SMB and ideacmdtool are part of the system software and cannot be easily updated, even with "advanced user" privileges. While it is possible to install a direct cable connection between the MaRS and the real-time processing laptop (see also Paret et al., 2018), this bypass may invalidate the CE (Conformité Européenne) certification of the MRI and is thus impractical for scanners used in clinical diagnostics. Here, researchers can adopt the interim solution described above.

Secondly, our observations in the "initial chaotic phase" (e.g., irregular absolute delays and display of mosaic images on the console monitor) suggest a bottleneck at the MaRS related to the computational cost of reconstructing the first image of the MB sequence. Researchers can shorten this period by adapting their protocol parameters (see Table 2), possibly at the expense of image quality such as reduced signal-to-noise ratio and temporal signal-to-noise ratio or increased inter-slice leakage artifacts as described elsewhere (Cauley et al., 2014). We have discussed the critical need for direct, delay-free real-time data transfer with the manufacturer. In the meantime, we hope that newer developments (e.g., Windows 10-based

operating systems such as syngo MR XA30 or new image reconstruction environments such as FIRE; Chow et al., 2021) will address these issues.

DATA AVAILABILITY STATEMENT

We make our procedure to determine the delay in image arrival times and the length of the chaotic initial phase, including the necessary code and SOP publicly available here: https://doi.org/10.11588/data/AIGXZZ.

ORCID

Malika P. Renz https://orcid.org/0000-0002-1334-3606
Jamila Andoh https://orcid.org/0000-0002-7088-0504
Mike M. Schmitgen https://orcid.org/0000-0002-6475-7155
Heike Tost https://orcid.org/0000-0002-7339-7569

REFERENCES

Bradley, M. M., & Lang, P. J. (2007). The international affective picture system (IAPS) in the study of emotion and attention. In *Handbook of emotion elicitation and assessment* (pp. 29–46). Oxford University Press.

Cauley, S. F., Polimeni, J. R., Bhat, H., Wald, L. L., & Setsompop, K. (2014). Interslice leakage artifact reduction technique for simultaneous multi-slice acquisitions. *Magnetic Resonance in Medicine*, *72*(1), 93–102.

Chow, K., Kellman, P., & Xue, H. (2021). Prototyping image reconstruction and analysis with FIRE. In SCMR 24th annual scientific sessions. Virtual Meeting.

Linhartova, P., Látalová, A., Kóša, B., Kašpárek, T., Schmahl, C., & Paret, C. (2019). fMRI neurofeedback in emotion regulation: A literature review. *NeuroImage*, *193*, 75–92.

Lührs, M., Poser, B., Auer, T., & Goebel, R. (2022). Retrieving fMRI data in real-time: Difficulties and pitfalls. *bioRxiv*. p. June 27, 2022.497807.

Oblak, E. F., Lewis-Peacock, J. A., & Sulzer, J. S. (2017). Self-regulation strategy, feedback timing and hemodynamic properties modulate learning in a simulated fMRI neurofeedback environment. *PLoS Computational Biology*, *13*(7), e1005681.

Paret, C., Zähringer, J., Ruf, M., Gerchen, M. F., Mall, S., Hendler, T., Schmahl, C., & Ende, G. (2018). Monitoring and control of amygdala neurofeedback involves distributed information processing in the human brain. *Human Brain Mapping*, *39*(7), 3018–3031.

Sitaram, R., Ros, T., Stoeckel, L., Haller, S., Scharnowski, F., Lewis-Peacock, J., Weiskopf, N., Blefari, M. L., Rana, M., Oblak, E., Birbaumer, N., & Sulzer, J. (2017). Closed-loop brain training: The science of neurofeedback. *Nature Reviews. Neuroscience*, *18*(2), 86–100.

SUPPORTING INFORMATION

Additional supporting information can be found online in the Supporting Information section at the end of this article.